Energy losses of positive and negative high-energy channeled particles

M. A. Hasan,* A. S. Kanofsky, and R. Allen†
Lehigh University, Bethlehem, Pennsylvania 18015

C. R. Sun, W. M. Gibson, I. J. Kim, and G. O. Williams
State University of New York, Albany, New York 12222

R. A. Carrigan, Jr., B. L. Chrisman, and T. E. Toohig
Fermi National Accelerator Laboratory, Batavia, Illinois 60510

Z. Guzik, T. S. Nigmanov, E. N. Tsyganov, and A. S. Vodopianov
Joint Institute for Nuclear Research, Dubna, U.S.S.R.

J. Kubic, D. H. Stork, and A. B. Watson
University of California, Los Angeles, California 90024
(Received 14 June 1982)

The results of measurements of energy losses of 35-, 100-, and 250-GeV particles channeled through a 2-cm Ge crystal are reported. The energy losses are correlated with the incoming and outgoing particle angles, relative to the channel axis, and the results are compared with existing theories.

INTRODUCTION

We report here on the energy loss of particles channeled through a 2-cm thick Ge crystal at energies of 35, 100, and 250 GeV. The theory of energy losses of particles passing through matter was first developed by Bohr, Bethe, and Bloch.[1] The theory of energy losses of channeled particles was developed to some extent by Lindhard in his seminal 1965 theoretical paper on particle channeling,[2] and more recently it has been dealt with in greater detail by Esbensen and Golovchenko.[3] We briefly present here an outline of the theory of energy loss and how it applies to channeled particles, the experimentally determined parameters of Lindhard's theory, and the minimum energy-loss values, and compare these with the theory of Golovchenko and Esbensen.

EXPERIMENTAL APPARATUS AND PROCEDURES

The channeling experiment was set up in the $M1$ beam line of the Fermi National Accelerator Laboratory in 1977. The data were taken for positive beam polarity at three different beam momenta, 35, 100, and 250 GeV/c, and negative beam polarity at 35 GeV/c only. The momentum spread, $\Delta p/p$, was less than 5%. The beam composition for the above-mentioned momenta and polarity configurations are listed in Table I.[4]

TABLE I. Beam composition for 35, 100, and 250 GeV/c momentum.

	Beam composition ($M1$ beam line, Meson Laboratory at Fermilab)		
	35 GeV/c %	100 GeV/c %	250 GeV/c %
π^+	88±1	62±1	6.7±0.4
K^+	5.8±0.7	5.1±0.7	1.75±0.05
p	6.8±1.0	31±1	92±1
π^-	92±1	93±1	97±1
K^-	5.4±0.7	5.4±0.7	2.35±0.05
$\bar{p}$	2.10±0.05	1.80±0.05	0.175±0.005

The experimental layout in the $M1$ beam line is shown in Fig. 1 (the dimension transverse to the beam is shown in an expanded scale). The germanium single crystal was mounted in the goniometer and placed 1 m downstream of the second Drift Chamber Module DC2. The first Drift Chamber Module DC1 was 31 m upstream and the third, DC3, was 17 m downstream of the crystal position. The Cerenkov counter C_k was upstream of DC1 and was used to discriminate between pions, kaons, and protons during parts of the experimental run. The vacuum pipes VP1 and VP2 were placed between the drift chamber modules to reduce multiple Coulomb scattering in air. They covered 91% of the space between the drift chambers.

The scintillation counter H had a 6-mm diameter hole that was centered on the crystal and partially covered it. It was placed between the second drift chamber and the crystal and was used to select particles that went through the crystal. The other scintillation counters $B0$, $B1$, $B2$, F, and W were used to define the beam particles, and to provide trigger pulses for the drift chambers.

The crystal was mounted in the goniometer and cooled to liquid-nitrogen temperature with the help of a copper cold-finger which was connected to the crystal with a flexible copper braid. A low pressure of $(3.0\pm0.2)\times10^{-6}$ Torr was maintained inside the goniometer chamber for all the experimental run.

The goniometer crystal mount was remotely controlled and had azimuthal and polar degrees of freedom with respect to the beam direction. It could be rotated independently in either direction in steps of 20 μrad. This step size, which is comparable to the halfwidth at half the maximum height (HWHM) of the axial channeling distribution at 250 GeV/c, was sufficient to align the crystal roughly along the beam direction. Accurate alignment was not necessary because the complete trajectory of the beam particle accepted in each event was recorded.

The three high-precision drift chamber modules were used to measure the position of each particle 31 and 1 m upstream and 17 m downstream of the crystal position. These drift chamber modules were originally built at the Joint Institute for Nuclear Research in Dubna, U.S.S.R.[5] They were further modified at Fermilab. The two upstream modules, DC1 and DC2, were of the same size, i.e., 12.5×12.5 cm^2, and the third downstream module was twice the size of the first and the second, i.e., 25×25 cm^2. Each module contained four X and four Y planes.

The Czochralski pulled germanium single crystal doped with 1×10^{10} phosphorous[6] was $20\times10\times8.5$ mm^3 in dimension. It was fabricated at Ortec into a transverse field intrinsic solid-state detector with boron-implanted p contact and lithium-diffused n contact on the opposite 10-mm long sides. The detector has oxide surface passivation and could be totally depleted at 50 V at the operating temperature of 128 °C or less.

The uncertainty in the alignment of the crystal face, cut perpendicular to the ⟨110⟩ axis, was less than 2°.

The signal from the crystal was fed into a conventional Nuclear Linear Electronics Amplifier system. This signal was proportional to the energy deposited by the charged particles passing through it. The crystal detector system was calibrated using ^{22}Na gamma-ray source having a gamma energy of 1.28 MeV. The resolution was found to be 10 keV full width at half maximum (FWHM).

A block diagram of the event trigger logic and data acquisition electronics is shown in Fig. 2. Beam particles were identified by a coincidence of $B1$, $B2$, F, and W with H (the scintillation counter with a hole) in anticoincidence. C_k was used in coincidence for some runs to identify pions. Signals from $B2'$ were discriminated in pulse height such that the large pulse heights due to two particles

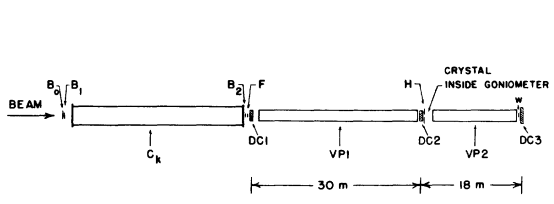

FIG. 1. Schematic illustration of the experimental setup. DC1–DC3 are drift chambers that define particle track. C_k is the Cerenkov counter that identifies the particle. The beam defining scintillation counters are B_0, B_1, B_2, F, H, and W. $VP1$ and $VP2$ are the vacuum pipes to reduce multiple scattering in air. The dimension transverse to the beam is shown in an expanded scale.

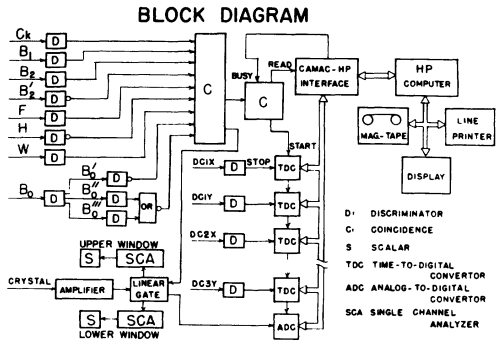

FIG. 2. The block diagram for the event trigger logic and data acquisition electronics.

passing through the scintillation counter at the same time produced a veto signal. This eliminated particles coming at the same time (i.e., in the same rf bucket).

By introducing proper delays in B_0, B_0'', and B_0''', all the particles arriving within the time interval of 500 nsec before and 80 nsec after the trigger pulse were vetoed. The final-event trigger logic was $C_k B_1 B_2 \bar{B}_2' F \bar{H} W B_0' (\overline{B_0''/B_0'''})$.

The event trigger pulse was used to gate the amplified signal from the crystal to the analog-to-digital converter (ADC) and to the two single-channel analyzers (SCA's). The two SCA's defined an upper and a lower window in the total pulse-height spectrum. The events falling in either of the two windows were counted and displayed on their respective scalars. The ratio of events falling in the two windows were used to locate the crystal axis, since particles traveling along the axis or crystal planes deposit less energy than those traveling along a random direction. Thus an increase in the ratio of lower window counts to upper window counts indicated alignment of a plane or axis along the beam direction.

The trigger pulse was also used to start the counting in all the time-to-digital converters (TDC's). The 48 active signal wires in the three drift chamber modules were each connected to a TDC through a discriminator. A signal, produced by the passage of a charged beam particle close to any of these wires, stopped the counting in the corresponding TDC. The other TDC's, corresponding to wires without particles passing by, would count to an overflow number.

The trigger pulse also initiated the transfer of data from the TDC's and ADC to the HP2100 computer through the interface and cleared all the TDC's and ADC for the next event. A small sample of the stored data in the computer could be analyzed on-line and displayed on the visual display for continuously monitoring the beam profiles, and, more importantly, the crystal alignment.

The alignment of the crystal was monitored by looking at the exit angle distribution of the particles with selection on small scattering angle and low energy loss. These selections should preferentially pick out channeled particles and a peak in the exit angle distribution should then be observed. The presence of this channeling peak at the same position would then indicate the proper alignment of the crystal.

The beam momentum was set to the desired value, 35 GeV/c, for positive particles by setting the currents in the beam dipole magnets to predetermined values. Adjustments were made in the focusing quadrupole magnets to make the beam as divergent as possible at the crystal position. This was necessary for crystal axis alignment. The broader the beam spread, the easier it was to bring the crystal axis position within the beam spread. Precise alignment and parallel beam were not required because, as mentioned before, the trajectory of each event particle could be obtained from the drift chamber data. The beam intensity per pulse was $\sim$20 k/pulse and the trigger logic accepted $\sim$300 events per pulse.

THEORETICAL DESCRIPTION AND RESULTS OF ENERGY LOSS

When a charged particle passes through a medium, it loses energy through elastic and inelastic collisions with the electrons and nuclei of the atoms in the medium. The nuclear collisions are very infrequent at very high energies of the beam particles. They are the source of the wide angle Rutherford elastic scatterings, and inelastic scatterings, and are responsible for depositing higher energies, in a single collision, in the medium. They contribute along with direct electron collisions to the long tail on the higher side of the distribution of energy deposited in the medium (Landau distribution).

The bulk of the energy loss of the beam particles in the medium is due to the large number of small scattering angle collisions with electrons. These collisions produce excitation and ionization of the electrons close to the path of the beam particle (close collisions). They also produce resonant excitation and ionization far from the particle path (distant collisions). The energy loss is divided between the close and the distant collisions. At higher energies, dE/dx is rising due to relativistic effects. However, the distant collisions are affected by the polarization of the medium, causing a decrease in the energy loss. This effect is more significant for dense material and is therefore called the "density effect."

The energy loss of relativistic charged particles incident on a crystal along a direction far away from any major crystal axes or planes (random direction), will be discussed first, and then the axial and planar channeling energy-loss results will be presented. In both cases, the density effect is important and will be included in the calculations.

CRYSTAL IN RANDOM ORIENTATION

The experimental energy-loss distribution for 250 GeV/c particles incident on the randomly oriented 2-cm thick Ge crystal is shown in Fig. 3 by the open circles. A random orientation is ideally a direction along which the crystal appears like an amorphous medium with atoms in random positions. For the

purpose of this experiment, a direction many times the critical channeling angle from any major low index axes and planar directions is considered as a random direction.

The excitations and ionizations by the incident particles of the electrons and the nuclei in the medium are statistical in nature. Consequently, the energy-loss values for particles traversing a material of a given thickness follow a statistical distribution. The sharp cutoff on the low-energy side is due to a minimum path length that the particles will have for a finite thickness of the medium. The long tail on the high-energy side is due to infrequent nuclear collisions (as mentioned before) and direct electron collisions.

The energy-loss distribution in an amorphous medium was obtained by Landau[7] by solving the transport equation for energy loss of charged particles in thin targets. The Landau distribution depends on a single parameter, and has the form

$$\varphi(\lambda)=\frac{1}{2\pi i}\int_{-i\infty}^{+i\infty} e^{u\ln(u)+\lambda u}du\ . \tag{1}$$

This integral has been evaluated by Borsch-Supan[8] for a wide range of values. The parameter λ is defined as

$$\lambda=\frac{\Delta E-\langle\Delta E\rangle}{\xi}-1-\beta^2+\gamma -\ln(\xi/T_{\max})\ , \tag{2}$$

where $\xi=2\pi Z_1^2e^4NZ_2t/mc^2\beta^2$, Z_1 and Z_2 are the atomic numbers of the incident particle and the target atom, respectively, N is the density of atoms in the target material, e is the electron charge, $\beta=v/c$, m is the mass of the electron, t is the thickness of the target, E is the actual energy loss, $\langle\Delta E\rangle$ is the mean energy loss, $\gamma=0.577216$ (Euler's constant),

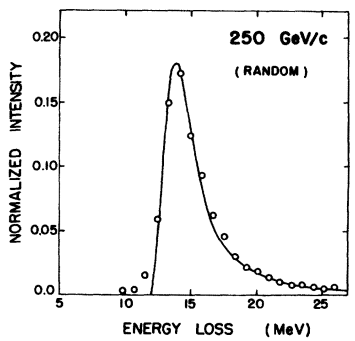

FIG. 3. Landau distribution for 250 GeV/c beam particles incident on 2-cm thick germanium crystal in random orientation. The open circles represent the experimental points.

and $T_{\max}$ is the maximum energy transferred to the electron in a head-on collision, i.e.,

$$T_{\max}=\frac{2mc^2\beta^2}{1-\beta^2}\left[1+\frac{2m}{M_1(1-\beta^2)}+\left[\frac{m}{M_1}\right]^2\right]^{-1}, \tag{3}$$

where M_1 is the mass of the incident particle. If the medium has finite thickness, then there is a large probability for the electrons, undergoing head-on collisions with relativistic particles, to come out of the medium without depositing all their energy in the medium (δ rays). For such a case, the logarithm term in the parameter has to be modified by replacing $T_{\max}$ with the value of the mean energy loss of the δ rays T_0 in the medium actually used.

For the purpose of fitting the Landau distribution to the experimental data, the experimental most probable energy-loss value $E_{\text{most probable}}$ was matched with the peak of the Landau distribution which occurs for $\lambda=-0.225$.

The fitted Landau curve is shown in Fig. 3 as a solid line. The experimental points fit the Landau distribution very well near the peak and the high-energy tail region.

The low-energy tail in the experimental distribution exists probably because of a combination of the following reasons. (1) There could be some high index axes and planes still present along the beam direction, i.e., the crystal was not aligned along a perfect random direction. (2) There could be two particles coming close in time and the amplifier remained dead for part of the time in the second particle's passage, thereby not collecting all the ions due to the second particle. (3) There could be some particles grazing the surface of the crystal.

The mean unrestricted dE/dx loss (stopping power) along a random direction in a dense medium has been given by Fano[9] as

$$\left\langle\frac{dE}{dx}\right\rangle=\frac{2\pi Z_1^2e^4NZ_2}{mc^2\beta^2}\left[\ln\frac{2mc^2\beta^2T_{\max}}{I^2(1-\beta^2)}-2\beta^2-\delta-\frac{2C}{Z_2}\right], \tag{4}$$

where I is the mean excitation energy of the target atoms, δ is the density effect contribution, and C is the shell correction. The other terms are the same as given previously. The shell correction for relativistic particles is small and was neglected for calculating $\langle dE/dx\rangle$ losses in this experiment.

As mentioned in the previous section, the knock-

on electrons (δ rays) do not deposit all their energy in the medium. Therefore, the maximum energy transferred to the electron T_{max} has to be replaced in Eq. (4) by the mean energy lost by the δ ray T_0. This yields the following formula for the mean restricted stopping power,[9] i.e.,

$$\left\langle \frac{dE}{dx} \right\rangle_{\text{restr}} = \frac{2\pi Z_1^2 e^4 N Z_2}{mc^2\beta^2} \left[\ln \frac{2mc^2\beta^2 T_0}{I^2(1-\beta^2)} - \beta^2 - \delta - \frac{2C}{Z_2} - \frac{(1-\beta^2)T_0}{2mc^2} - \Delta C \right], \tag{5}$$

where ΔC is a small correction factor of the order of 1 for gases and 0.01 for solids. This correction factor was also neglected in the calculation of the mean restricted stopping power (along with the shell correction). Sternheimer and Peierls[10] give the most probable stopping power as

$$\left[\frac{dE}{dx} \right]_{\text{most prob}} = \frac{2\pi Z_1^2 e^4 N Z_2}{mc^2\beta^2} \left[\ln \frac{4\pi Z_1^2 e^4 N Z_2 t}{I^2(1-\beta^2)} - \beta^2 - \delta + 0.198 \right]. \tag{6}$$

The mean energy loss of the δ rays is apparently accounted for by the constant factor, 0.198.

The density effect correction δ in the above three expressions for stopping power was obtained from the following parametric equations[11]:

$$\delta(X) = 4.606X + C + a(X_1 - X)^m, \quad (X_0 < X < X_1)$$

$$\delta(X) = 4.606X + C, \quad (X > X_1) \tag{7}$$

and

$$X = \log_{10}\left[\frac{P}{M_1 C} \right],$$

where C, a, X_0, X_1, and m are parameters whose values for many common substances have been listed in Ref. 11. For germanium the values of these parameters are $C = -5.10$, $a = 0.1666$, $m = 3.136$, $X_0 = 0.10$, and $X_1 = 3.0$.

A rough estimate of the mean excitation energy is obtained from $I = 10Z_2$ eV which for germanium yields 320 eV. A more accurate value, $I = 340 \pm 10$ eV, has been recommended by Ahlen[12] and was used in calculating the stopping powers. The mean energy deposited by the δ rays T_0 in the 2-cm thick germanium crystal was estimated in the following manner.

The energetic δ-ray electrons were scattered mostly in the forward direction. It was therefore assumed that all the energetic knock-on electrons came out of the back end of the crystal. It was also assumed that the δ rays of energy T are produced with equal probability throughout the crystal. The production probability of the δ rays of energy T is given by[13]

$$\frac{dN}{dT\,dx} \simeq \frac{2\pi Z_1^2 e^4 N Z_2}{mc^2\beta^2} \frac{1}{T^2} \tag{8}$$

for $I \ll T < T_{max}$.

The energy deposited by a δ ray of energy T produced at a distance x from the back end of the crystal was obtained by dividing the thickness x into strips of width 0.1 cm and calculating the energy deposited in successive strips from the tabulated stopping powers of electrons.[13] Using the probability expression of Eq. (8) and the energy deposited by the δ rays produced at different depths in the crystal, an average energy loss was found. For a 2-cm thick germanium crystal, the average energy loss of the δ rays was $T_0 = 5.23$ MeV for 35, 100, and 250 GeV/c beam particles. Although the method outlined above for estimating T_0 is very crude, an error of 30% in the T_0 value would produce an error of only 1% in the mean restricted stopping power, i.e., the mean restricted stopping power is not sensitive to the exact value of T_0. However, the correction due to the mean energy deposited by the δ rays T_0 is important, because the T_{max} value it is supposed to replace in the stopping power formula is 2–4 orders of magnitude higher than the T_0 value.

The most probable, the mean restricted, and the mean unrestricted stopping powers of the composite beam of protons, pions, and kaons, incident on a 2-cm-thick germanium crystal, oriented in a random direction, were calculated for relativistic momenta in the range of 5–300 GeV/c using the formulas given above. A weighted average of the stopping powers, using the percentage composition of the beam particles from Ref. 4, was found for each beam momentum value. The maximum difference in the mean stopping power was 2% for 35 GeV/c pions and protons.

The above-mentioned stopping powers are shown by solid curves in Fig. 4. The experimentally observed values of the mean restricted stopping power and the most probable stopping power are indicated by circles and triangles in the figure, respectively.

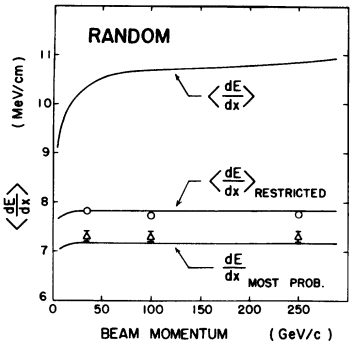

FIG. 4. Comparison of the theoretical and experimental values of the restricted mean and most probable energy loss in 2-cm thick randomly oriented germanium crystal. The unrestricted mean energy-loss curve is also drawn. The open circles and triangles are the experimental values of the restricted mean and most probable energy losses, respectively.

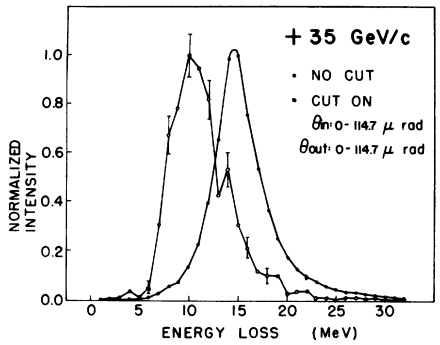

FIG. 5. The normalized energy-loss distributions of channeled (open circles) and random (solid circles) particles (35 GeV).

The theoretical and experimental values of the stopping powers are also listed in Table II.

There is very good agreement between the theoretically calculated values and the experimental fitted results. This also shows that the estimate of the mean energy loss of the δ rays T_0 was reasonable.

The fact that the mean stopping power $\langle dE/dx \rangle$, with no correction for the δ rays, is 40% higher than the restricted mean stopping power $\langle dE/dx \rangle_{\text{restr}}$, with δ-ray corrections applied, indicates that the δ-ray correction is very important for high-energy beams penetrating a crystal of finite thickness.

CRYSTAL ORIENTED ALONG ⟨110⟩ AXIS DIRECTION

The positively charged beam particles that enter the crystal at an angle less than the critical angle with respect to the axis direction are steered away from the high-density regions. The close collision probability with the electrons is greatly reduced, but the resonant excitation and ionization probability of the distant electrons remain unchanged in comparison to the random orientation case. The density effect will therefore be the same for the axial as well as the random orientation of the crystal.

Nuclear collisions are even more negligible for channeled particles than for random particles since they do not approach close to atoms in the crystal. This reduced electronic and nuclear collision probability for the channeled particles will produce a reduction in the energy deposited in the crystal.

The energy-loss distribution of the channeled particles at 35, 100, and 250 GeV/c beam momenta are shown in Figs. 5, 6, and 7, respectively. The open represent the distributions for channeled particles and were obtained by selecting particles that were within the critical angle in the incident and the exit projected angle plane with respect to the ⟨110⟩ axis direction. The solid dots represent distributions with no selection and are primarily the random energy-loss distribution.

The small peak on the high-energy side of the 35 GeV/c channeled particle energy-loss distribution is at the same position as the most probable energy loss for random orientation. This suggests that there is perhaps some contamination from random particles. The contamination is seen as a shoulder in the channeled particle energy-loss distribution at 100 GeV/c beam momentum. It is practically absent in the 250 GeV/c data.

The decrease of error in the angle measurement with increasing energy of the beam and the fact that the selections on the incident and exit angles were applied is a strong indication that the random parti-

TABLE II. Experimental and theoretical values of the mean restricted stopping power and most probable stopping power for particles passing through a randomly oriented crystal.

(MeV/cm)		35 GeV/c	100 GeV/c	250 GeV/c
$(dE/dx)_{\text{restr}}$	Experimental	15.7±0.1	15.5±0.1	15.5±0.1
	Theoretical	15.61	16.63	16.65
$(dE/dx)_{\text{most prob}}$	Experimental	14.6±0.2	14.6±0.2	14.6±0.2
	Theoretical	14.33	14.35	14.36

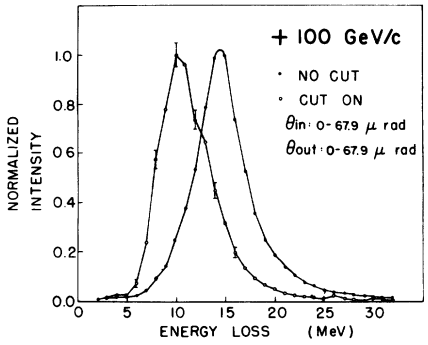

FIG. 6. The normalized energy-loss distributions of channeled (open circles) and random (solid circles) particles (100 GeV).

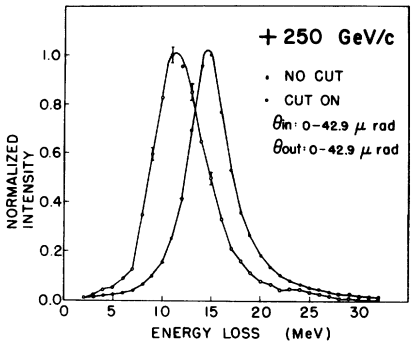

FIG. 7. The normalized energy-loss distributions of channeled (open circles) and random (solid circles) particles (250 GeV).

cle energy-loss component may be due to the resolution in the incident and the exit angle measurement. Since the error in the angle measurement is largest at 35 GeV/c momentum, therefore, the random component of the energy loss is also maximum at this momentum value.

Various authors (Refs. 14, 15, and 3) have proposed different mechanisms to calculate the stopping power of the channeled particles as a function of impact parameter $\vec{b}$ in the transverse plane.

The results of this experiment agree well with Esbensen and Golovchenko's calculation.[3] They calculate the energy loss of the fast-channeled particles on the basis of quantum perturbation methods. Their result, modified to include relativistic particles, is

$$\left\langle \frac{dE}{dx}(\vec{b}) \right\rangle = \frac{2\pi Z_1^2 e^4 N}{mc^2\beta^2}\left[[Z_2+Z(\vec{b})]\ln\left[\frac{2mc^2\beta^2}{I(1-\beta^2)}-\beta^2\right]-Z_2\delta+C(\vec{b})\right], \tag{9}$$

where K is the reciprocal lattice vector in the transverse space and $Z(\vec{b})$ is the average electron density at $\vec{b}$,

$$C(\vec{b})=\sum_{\vec{K}\neq 0} e^{i\vec{K}\cdot\vec{b}}\ln\left[\frac{2mI}{\hbar^2K^2}\right]\rho(\vec{K})$$

and

$$\rho(\vec{K})=\langle 0\,|\,e^{-i\vec{K}\cdot\vec{r}}\,|\,0\rangle\ . \tag{10}$$

The last term $\rho(\vec{K})$ is the Fourier transform of the electronic charge density in the target atom in its ground state. It is also known as the atomic form factor.

Doyle and Turner[16] have given an eight-parameter equation to calculate the atomic form factors of all the elements except hydrogen. The average electron density $Z(\vec{b})$ in the transverse space is obtained by taking the inverse Fourier transform of the atomic form factor in the transverse reciprocal lattice space, i.e.,

$$Z(\vec{r})=\sum_{\vec{K}} e^{i\vec{K}\cdot\vec{r}}\rho(K)\ . \tag{11}$$

The comparison of the mean stopping power of Eq. (9) as a function of impact parameter with the experimental results was difficult to obtain for individual values of $\vec{b}$. This was because it was not possible to isolate experimentally the particles with a single impact-parameter value.

A measure of the energy loss of best-channeled particles could nevertheless be obtained from the channeled particle energy-loss distribution and compared with the theoretical prediction of Eq. (9). The best-channeled particles were defined as the particles going through the center of the channel. For the $\langle 110\rangle$ axis in the germanium crystal, the center of the channel is equidistant from the six closest strings of atoms, and the distance is $b=2.122$ Å.

The distributions of the energy loss of 100 GeV/c beam particles along the $\langle 110\rangle$ axis in the germanium crystal are shown in Fig. 8. The open triangles and the open circles represent the distributions with selections on incident angle of 0 to 45 μrad and 0 to 75 μrad, respectively. The two distributions have zero incident angle with respect to the $\langle 110\rangle$ axis direction in common, and consequently they contain the best-channeled particles.

The extrapolated intercepts on the low-energy side of these two distributions lie at the same point (within experimental error). This type of behavior is also observed in the 35 and 250 GeV/c data. This

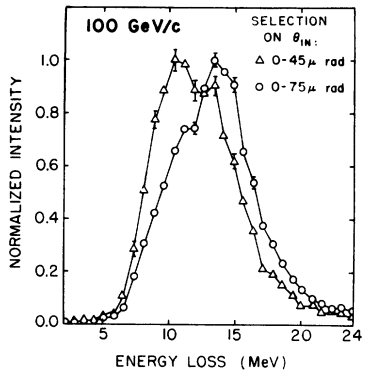

FIG. 8. Normalized energy-loss distribution for two different selections on the incident angle.

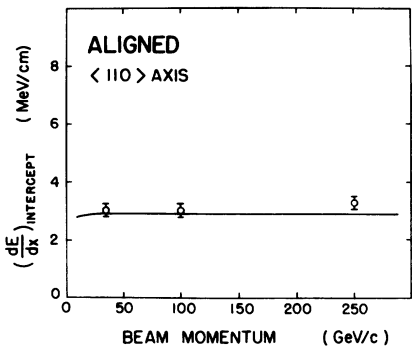

FIG. 9. The stopping power at the intercept value on the low-energy side of the energy-loss distribution for channeled particles. The solid line is the theoretical curve and the open circles are the experimental values.

shows that the intercept of the channeled particle energy-loss distribution is not too sensitive to the selections on the incident angle, as long as the best-channeled particles are included in the selection. Therefore, the intercept value on the low-energy side of the channeled particles energy-loss distribution was used for comparison with Esbensen and Golovchenko's calculation.[3]

It was assumed that the energy loss of the best-channeled particles follow the Landau distribution. The stopping power corresponding to the intercept value was then obtained from the mean stopping power of Eq. (9) by using the Landau distribution parameter, defined in Eq. (2). The value for the intercept on the low-energy side of the Landau distribution is -2.5. With this value in Eq. (2) one obtains

$$\left[\frac{dE}{dx}(\vec{b})\right]_{\text{intercept}} = \left\langle \frac{dE}{dx}(\vec{b}) \right\rangle + \frac{\xi}{t}\left[-1.077+\ln\left[\frac{\xi}{T_{\max}}\right]\right], \tag{12}$$

where $\xi = 2Z_1^2 e^4 N Z_2(\vec{b})/mc^2\beta^2$ and the other quantities have already been defined in previous sections. The intercept value of the stopping power, as calculated from Eq. (12), with the mean energy loss of the well-channeled particles obtained from Esbensen *et al.*,[17] is plotted as a solid line in Fig. 9. The experimental points are shown as open circles, and they agree well with the predicted values. The experimental and the calculated values at the three beam momenta are given in Table III.

It may be pointed out here that the authors of Ref. 17 take the position of half the peak value on the low-energy side of the channeled particle energy-loss distribution as the reference point to compare their results with the theory. Since they had many more events in each configuration as compared to this experiment, they could apply stricter selections on the incident and exit angle and thereby eliminate almost completely the random component in the channeled particle energy-loss distribution. Under those conditions they found that the position of half the peak value on the low-energy side of the channeled particle energy-loss distribution was not sensitive to selections on the incident and exit angles. They calculated the stopping power corresponding to half the peak value on the low-energy side from Eqs. (9) and (2) with $\lambda = -1.6$.

Lindhard, in his famous 1965 paper on channeling[2] has derived expressions for the electronic and the nuclear stopping power as a function of the incident angle with respect to the crystal axis direction. He has suggested that the nuclear stopping power will be very small compared to the electronic stopping power for particles with relativistic velocities. This difference will be even greater for channeled particles because of the absence of nuclear collisions for the best-channeled particles. Therefore, the electronic stopping power for the channeled particles will be considered and the nuclear stopping power will be disregarded.

Lindhard gives the following form for the mean electronic stopping power as a function of the incident angle:

TABLE III. Low-energy zero-value intercept experimental and theoretical values.

$(dE/dx)_{\text{intercept}}$ (MeV/cm)	35 GeV/c	100 GeV/c	250 GeV/c
Experimental	3.06±0.20	3.05±0.20	2±0.20
Theoretical	2.90±0.02	2.91±0.02	2.91±0.02

$$\left\langle \frac{dE}{dx}(\theta_{\text{in}}) \right\rangle_e = \left\langle \frac{dE}{dx} \right\rangle_e (1-\alpha e^{2\theta_{\text{in}}^2/\psi_1^2}) , \quad (13)$$

where ψ_1 is the Lindhard critical angle defined as $(2Z_1Z_2e^2/dE)^{1/2}$, $\langle dE/dx \rangle_e$ is the electronic stopping power for random orientation of the crystal, and α is a constant whose value was suggested by Lindhard to be between $\frac{1}{2}$ and 1.

Since the nuclear stopping power is neglected, the total mean stopping power has the same form as Eq. (13). The mean energy loss for the beam particles in a finite thickness of the crystal will then be given by

$$\langle \Delta E(\theta_{\text{in}}) \rangle = \langle \Delta E \rangle (1-\alpha e^{-2\theta_{\text{in}}^2/\psi_1^2}) . \quad (14)$$

A curve of the functional form of Eq. (14) was fitted to the experimental data of the mean energy loss versus the incident angle (θ_{in}) at 35, 100, and 250 GeV/c beam momenta. These are shown in Figs. 10, 11, and 12, respectively. The values obtained for the parameters are given in Table IV. The curve fitting is best for the 250 GeV/c data and worst for the 35 GeV/c data as can be seen from the χ's values. The worse fit for 35 GeV/c momentum was due to the angular resolution of the system being substantially poorer (47 μrad at 35 GeV) than at the higher momenta.

The general behavior of the energy loss as a function of the incident angle with respect to the axis direction follows Lindhard's prediction quite well to the highest momentum of the beam particles in this experiment except that the fitted value of the parameter α is less than the range suggested by Lindhard. The parameter values are essentially unchanged with energy.

CRYSTAL ORIENTED ALONG (111) PLANAR DIRECTION

The energy-loss distributions for planar channeling of 35 and 250 GeV/c particles are shown in Figs. 13 and 14, respectively. The solid circles represent the distributions with no selection on incident angle. The open circles represent the distributions with a selection on the Y component of the incident angle around the origin, which is along the (111) planar direction in the crystal. A selection on the Y component of the scattering angle, $\Delta\theta_Y$, was also applied. The range of the selections for the two beam momenta values are indicated in the figures. These two selections were applied in combination, to pick out as many well-channeled particles as possible and at the same time have enough events to get statistically significant results.

Since the multiple-scattering resolution of the system is of the same order of magnitude as the planar channeling distribution halfwidths $\psi_{1/2}$, there was a large contamination of the random beam particle energy-loss distribution.

It was explained in detail earlier that the intercept value on the low-energy side of the energy-loss distribution of the channeled particles could be used for comparison with the theoretical predictions. These intercept values were obtained from the shoulders of

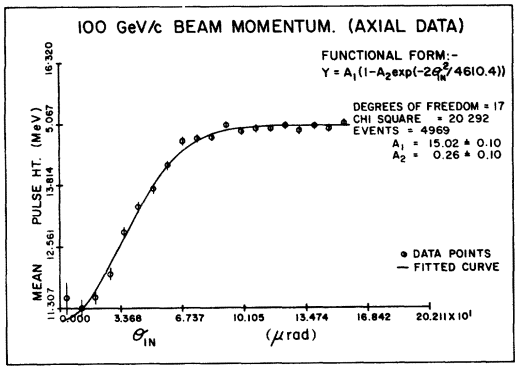

FIG. 11. Curve fitting of Lindhard's functional form of the mean energy loss as a function of the incident angle (100 GeV/c).

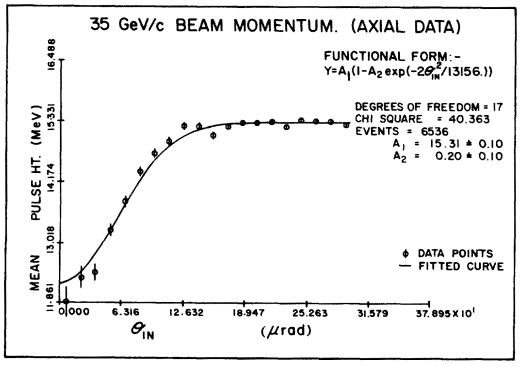

FIG. 10. Curve fitting of Lindhard's functional form of the mean energy loss as a function of the incident angle (35 GeV/c).

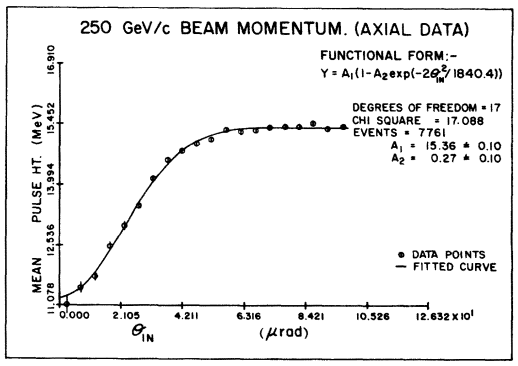

FIG. 12. Curve fitting of Lindhard's functional form of the mean energy loss as a function of the incident angle (250 GeV/c).

TABLE IV. Values of χ^2 and the parameters obtained from fitting the Lindhard formula for the mean electronic stopping power $[\langle \Delta E \rangle (1-\psi e^{-2\theta_{in}^2/\psi_1^2})]$ to the data.

	35 GeV/c	100 GeV/c	250 GeV/c
$\langle \Delta E \rangle$ (MeV)	15.31±0.67	15.02±0.69	15.36±0.57
α	0.20	0.26	0.27
$\chi^2(N_D=17)$	40.4	20.3	17.1

the channeled particles energy-loss distributions in Figs. 13 and 14. The stopping powers corresponding to the intercept value of the energy loss were compared to the calculations of Esbensen and Golovchenko using the same technique as used for the energy loss of the axially channeled particles described earlier.

The calculated and the experimental values are listed in Table V.

From these numbers one can see that there is good agreement between the Esbensen and Golovchencko calculations and the experimental results.

LARGE ENERGY LOSSES DUE TO NUCLEAR COLLISIONS

It is worth noting that nuclear collisions should result in large energy losses. Thus it is expected that nuclear collision "blocking" and multiparticle production events would result in large energy losses. Such is the case, and the results are described in a previous paper[18] and one to follow.

NEGATIVE-PARTICLE ENERGY LOSSES

The experimental data and theory for the channeling of positive particles is fairly complete, while very little is known either experimentally or theoretically about the channeling of negative particles. Before the advent of high-energy GeV particle channeling experiments, it was necessary to use electrons of MeV energies as the channeled particles, which complicated matters because of the long wavelength of electrons at this energy and the consequent quantum interference effects that occur with the lattice, which are well known to people who study electron diffraction scattering. As well, the light mass of the electron results in larger multiple-scattering effects.

We report here on the energy losses of negative pions of 35 GeV energy.

The behavior of the negatively charged beam particles is expected to be different from that of the positively charged particles, when they are interacting with rows of atoms along a channeling axis direction. Whereas the positive particles are steered away from the higher potential regions of the rows of atoms, the negatively charged particles are attracted towards them. This leads to an increase in the probability for physical processes involving small impact-parameter collisions, such as large-angle Rutherford scattering, nuclear reactions, multiple scattering, x-ray production, etc. This is in contrast to a decrease in such processes for positively charged particles.

The increase in large-angle scattering processes will lead to a broad dip in the transmission yield of the negative particles in the exit angle plane around the axis direction. However, the particles that are

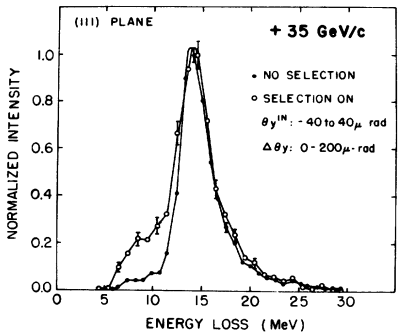

FIG. 13. Normalized energy-loss distribution for 250 GeV/c beam momentum. The selections are indicated in the figure.

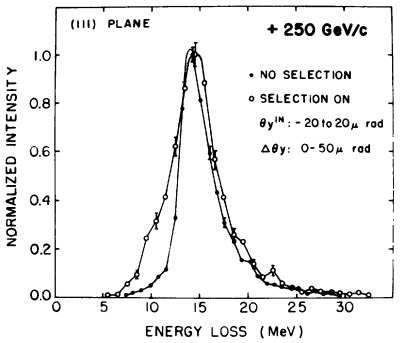

FIG. 14. Normalized energy-loss distribution for 35 GeV/c beam momentum. The selections are indicated in the figure.

TABLE V. Stopping powers of the intercept value of the energy loss compared to the calculations of Esbensen and Golovchenko.

$(dE/dx)_{\text{intercept}}$	35 GeV/c	250 GeV/c
Experimental	2.7±0.3	3.1±0.3
Calculated	2.99±0.05	3.15±0.05

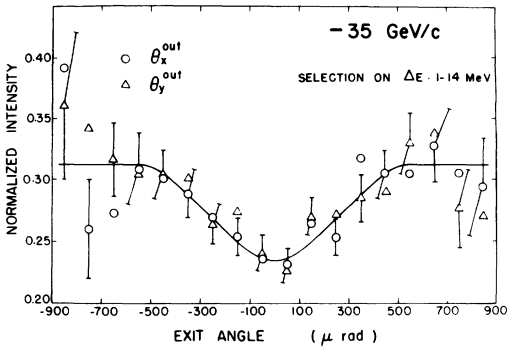

FIG. 15. Exit angle distribution of -35 GeV/c beam particles around the $\langle 110 \rangle$ axis. The $\langle 110 \rangle$ axis is at the origin of the exit angle axis.

incident at small angle to the $\langle 110 \rangle$ axis direction and have large angular momentum with respect to the axis direction will stay away from the high-density regions of rows of atoms. This is due to the repulsive angular momentum term which causes the particles to spiral around one string of atoms as they pass through the crystal. This will lead to a decrease in large-angle scattering of the beam particles with such angular momentum and therefore a peak in the middle of the broad dip is expected to be observed in the exit plane. This type of behavior has been observed for negative particles at lower energies.[19] The width of the dip was three to four times the critical angle.

In our experiment, the projected exit angle distribution with a selection of 1 to 14 MeV on energy loss showed a broad dip around the $\langle 110 \rangle$ axis (Fig. 15). The low-energy loss selected on particles that did not approach the string too closely. This broad dip indicates that most of the particles undergo small impact-parameter collisions with the string

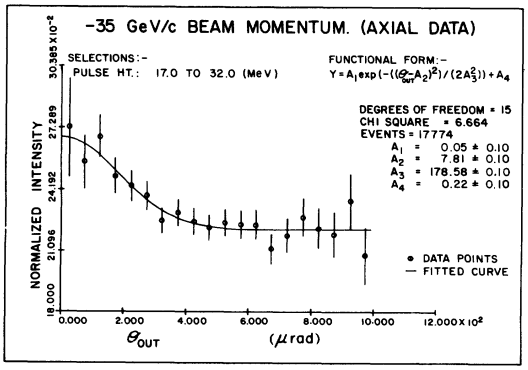

FIG. 16. Normalized exit angle distribution with selection on energy loss. A Gaussian is fitted to the distribution to extract its width.

TABLE VI. Values of the fitted channeled HWHM values (for a Gaussian) of positive and negative particles at 35 GeV/c momentum.

$\psi_{1/2}\langle 110 \rangle$	$+35$ GeV/c	-35 GeV/c
μrad	45.22	210.18

when they are incident at small angles to the crystal axis direction. The predicted peak in the center of the broad dip was not observed probably because of the poor statistics of the data and poor angular resolution of the apparatus.

Since there is no comprehensive theory of negative-particle behavior in the axial channeling region as there is for positive particles (Lindhard's theory), a qualitative comparison was made between the behavior of the negative and the positive particles at 35 GeV/c beam momentum, and these are presented in the following section.

The negative particles that are incident at small angles to the $\langle 110 \rangle$ axis in the crystal are attracted towards the positively charged nuclei in the string of atoms along the axis direction. These particles spend more time in the high-density regions near the center of the string in the transverse plane and therefore lose more than average energy in the crystal. The particles that go along the channeling axis direction may therefore be identified by their energy loss. A greater proportion of particles going along the channeling axis direction would be contained among particles which have higher than average energy loss. This is also seen in the energy-loss spectrum of the negative particles given later.

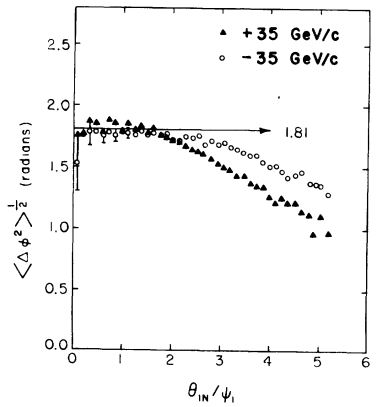

FIG. 17. The rms azimuthal scattering angle distribution for -35 GeV/c (open circles) and $+35$ GeV/c (solid triangles) data. The theoretically expected value of 1.81 for equilibrium in the azimuthal scattering angle is also indicated.

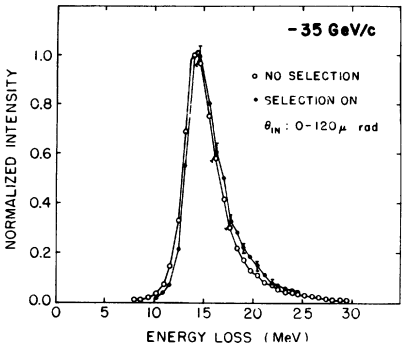

FIG. 18. Normalized energy-loss distribution for -35 GeV/c particles. The selections are indicated in the figure.

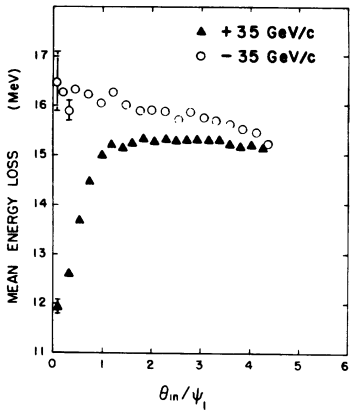

FIG. 19. Mean energy loss of 35 GeV/c positive (solid triangles) and negative (open circles) particles as a function of the scaled incident angle.

Negative particles with energy loss in the range of 17–32 MeV were selected and their normalized distribution in the exit angle is shown in Fig. 16. The distribution was normalized by dividing the data with a similar distribution with no selection applied. An enhancement in the intensity was observed near the channeling axis direction, which is at the origin of the exit angle axis. A Gaussian curve was fitted to the distribution and the halfwidth at half maximum value $\psi_{1/2}\langle 110\rangle$, was extracted from the fitted parameters. The values of $\psi_{1/2}\langle 110\rangle$ for the negative and positive particles are given in Table VI.

The $\psi_{1/2}\langle 110\rangle$ value for the negative particles is ~ 4.5 times that of the positive particles. This is consistent with the broad width observed for the negative-particle distribution in other experiments.

The rms distribution of the azimuthal scattering angle for -35 GeV/c (open circles) and $+35$ GeV/c data (solid triangles) is shown in Fig. 17. The predicted value of 1.813 for statistical equilibrium in the azimuthal angle is indicated as well.

The energy-loss distribution for the negative particles is shown in Fig. 18. The open circles represent data with no selection, and the solid circles the distribution with selection on the incident angle of zero to 120.0 μrad.

The distribution with selection, which represents negative particles incident at small angles to the string direction, shows a slight shift towards higher energy loss. This is expected because of the attractive nature of the string potential for negative particles, which leads to an increase in the fraction of time that the particles spend in the high-density (electron and nuclear) regions of the crystal and therefore an increase in the energy loss.

The mean energy loss of the positive and the negative particles as a function of the scaled incident angle is shown in Fig. 19. This clearly shows the marked difference in the behavior of the positive- and the negative-channeled particles.

The mean energy loss actually increases for negative particles when the particles are incident within the critical angle region. In contrast, the positive particles show a significant decrease in the mean energy loss for particles incident close to the $\langle 110\rangle$ axis direction.

ACKNOWLEDGMENTS

We would like to thank the members of the Dubna-Fermilab-Notre Dame-Pittsburgh-UCLA form-factor experiment for letting us use their apparatus and helping to acquaint us with its operation. A. Wehmann and M. Atac have been particularly helpful. We would also like to express our thanks to the Directorate and Staff at Fermilab for permitting us to perform this experiment in conjunction with the form-factor experiment. This work was funded in part by Lehigh University and the U. S. Department of Energy under Contract No. DE-AC02-76ER02894, A004.

*Present address: Department of Physics, University of Wisconsin, Madison, Wisconsin 53706.

†Present address: Department of Physics, University of California, Irvine, California 92717.

[1]N. Bohr, Philos. Mag. 25, 10 (1913); 30, 581 (1915); H. A. Bethe, Ann. Phys. 5, 325 (1930); F. Bloch, Z. Phys. 81, 363 (1923).

[2]J. Lindhard, K. Dan. Vidensk. Selsk. Mat.-Fys. Medd.

34, 1 (1965).

[3]H. Esbensen, O. Fich, J. A. Golovchenko, K. O. Nielsen, E. Uggerhoj, C. Vraast-Thomsen, A. Charpak, S. Majewski, F. Sauli, and J. P. Ponpon, Nucl. Phys. B127, 281 (1977); H. Esbensen and J. A. Golovchenko, *ibid.* A298, 383 (1978).

[4]W. F. Baker, A. S. Carroll, I-H. Chiang, D. P. Eartly, O. Fackler, G. Giacometti, A. M. Jonckheere, P. F. M. Koehler, T. F. Kycia, K. K. Li, M. O. Marx, P. O. Mazur, D. C. Rahm, and R. Rubinstein, Fermi internal report, Fermilab Report No. 78/79, EXP7110-104 (unpublished).

[5]N. A. Filatova, T. S. Nigmanov, V. P. Pugachevich, V. D. Riabstov, M. D. Shefranov, E. N. Tsyganov, D. V. Uralsky, A. S. Vodopianov, F. Sauli, and M. Atac, Fermilab Report No. 76/97, EXP7500-456 (unpublished).

[6]D. T. J. Hurle and Ed. P. Hartman, in *Crystal Growth: A Tutorial Approach,* Proceedings of the 3rd International Summer School, 1977, edited by W. Bardsley, D. T. J. Hurle, and J. B. Mullin (North-Holland, Amsterdam, 1979).

[7]L. Landau, J. Exp. Phys. (USSR) 8, 201 (1944).

[8]W. Borsch-Supan, J. Res. Natl. Bur. Stand. 65B, 245 (1961).

[9]V. Fano, Annu. Rev. Nucl. Sci. 13, 67 (1963).

[10]R. M. Sternheimer, Phys. Rev. B 3, 3681 (1971).

[11]R. M. Sternheimer, Phys. Rev. 145, 247 (1966).

[12]S. P. Ahlen, Rev. Mod. Phys. 52, 121 (1980).

[13]M. J. Berger and S. M. Seltzer, *Studies in Penetration of Charged Particles in Matter,* National Research Council, National Academy of Sciences, Report No. 1133, 1964 (unpublished).

[14]V. V. Beloschitsky and M. A. Kumakov, Radiat. Eff. 35, 209 (1978).

[15]K. Dettmann and M. T. Robinson, Phys. Rev. B 10, 1 (1974).

[16]P. A. Doyle and P. S. Turner, Acta Crystallogr. Sect. A 24, 390 (1968).

[17]H. Esbensen *et al.*, Phys. Rev. B 18, 1039 (1978).

[18]R. A. Carrigan, Jr., B. L. Chrisman, T. E. Toohig, W. M. Gibson, Ick-Jon Kim, C. R. Sun, Z. Guzik, T. S. Nigmanov, E. N. Tsyganov, A. S. Vodopianov, M. A. Hasan, A. S. Kanofsky, R. Allen, J. Kubic, D. H. Stork, and A. B. Watson, Nucl. Phys. B163, 1 (1980).

[19]For a review of electron channeling see, e.g., D. S. Gemmel, Rev. Mod. Phys. 46, 129 (1974). Lower energy channeling of negative pions is reported in the following papers. H. Esbensen, O. Fich, J. A. Golovchenko, K. O. Nielsen, E. Uggerhøj, C. Vraast-Thomsen, G. Charpak, S. Majewski, F. Sauli, and J. P. Ponpon, Nucl. Phys. B127, 281 (1977); H. Esbensen, O. Fich, J. A. Golovchenko, S. Madsen, H. Nielsen, H. E. Schiott, E. Uggerhøj, C. Vraast-Thomsen, G. Charpak, S. Majewski, G. Odyniec, G. Petersen, F. Sauli, J. P. Ponpon, and P. Siffert, Phys. Lett. 72B, 408 (1978).